RESEARCH ARTICLE

MEMBRANES

Large-area graphene-nanomesh/carbon-nanotube hybrid membranes for ionic and molecular nanofiltration

Yanbing Yang[1]*, Xiangdong Yang[2]*, Ling Liang[3], Yuyan Gao[4], Huanyu Cheng[4], Xinming Li[5], Mingchu Zou[6], Anyuan Cao[6], Renzhi Ma[5], Quan Yuan[1,3]†, Xiangfeng Duan[7]†

Nanoporous two-dimensional materials are attractive for ionic and molecular nanofiltration but limited by insufficient mechanical strength over large areas. We report a large-area graphene-nanomesh/single-walled carbon nanotube (GNM/SWNT) hybrid membrane with excellent mechanical strength while fully capturing the merit of atomically thin membranes. The monolayer GNM features high-density, subnanometer pores for efficient transport of water molecules while blocking solute ions or molecules to enable size-selective separation. The SWNT network physically separates the GNM into microsized islands and acts as the microscopic framework to support the GNM, thus ensuring the structural integrity of the atomically thin GNM. The resulting GNM/SWNT membranes show high water permeance and a high rejection ratio for salt ions or organic molecules, and they retain stable separation performance in tubular modules.

Water desalination and purification is an attractive pathway to fresh water because seawater represents the largest fraction of water on Earth (*1*, *2*). An ideal water-treatment membrane should exhibit several critical characteristics: (i) minimal thinness to maximize permeance (*3*, *4*); (ii) sufficient mechanical strength to avoid breakage and solute leakage (*5*–*7*); and (iii) uniform and narrow pore size distribution for efficient separation (*8*, *9*). To this end, nanoporous two-dimensional (2D) materials of single- or few-atom thickness and with excellent mechanical strength have been considered as the ideal building blocks for constructing ultrathin membranes with minimum transport resistance and maximum permeance (*10*–*14*). Theoretical calculations have predicted that single-layer nanoporous 2D membranes can provide ultrafast water permeation and selective separation (*15*, *16*). Experimental studies of nanoporous graphene membrane have also demonstrated its exceptional performance in water desalination. However, the experimental studies to date are typically limited to proof-of-concept demonstrations on micrometer-scale graphene flakes (10^{-6} to 10^{-8} cm^2).

Although defect-free graphene exhibits exceptional mechanical performance, the inevitable in-plane grain boundaries in large-area graphene could seriously weaken the mechanical strength, and the introduction of pores could further compromise the structural integrity of single-layer graphene (*17*, *18*). Because the desalination process relies on the molecular-level separation of solute ions from water molecules, any slight tearing or cracking of the membrane could undermine the entire desalination system. As the stress of a selective membrane scales with $d^{-3/2}$ (where d is the membrane thickness), the atomically thin 2D membrane that is three orders of magnitude thinner than the commercial membrane would undergo substantially larger stress (*19*). Therefore, the applications of ultrathin 2D membranes for practical water treatment remain rather elusive because of the challenges in reliably producing large-area nanoporous 2D membranes of sufficient mechanical strength.

We report the design of an atomically thin nanoporous membrane with a single-layer graphene nanomesh (GNM) supported by an interwoven network of single-walled carbon nanotubes (SWNTs) (Fig. 1). In this structure, the mechanically strong, interconnected SWNT webs (*20*) feature a strong π–π interaction with the supported GNM, physically separate the GNM into microsized islands, and act as a microscopic framework to support the GNM (Fig. 1A). This construct can be viewed as Voronoi cells (*21*, *22*) of a Voronoi diagram (for example, as commonly seen in insect wings or plant leaves; fig. S1) defined in the mathematical structure models, thus ensuring the structural integrity of the atomically thin GNM over macroscopic scale. The large-area, ultrathin GNM/SWNT hybrid membrane can serve as an excellent size-exclusion nanofiltration membrane. In particular, the high-density subnanometer pores in the GNM layer allow efficient transport of water molecules with minimum resistance while blocking solute ions or molecules to enable selective separation (Fig. 1B), and the high mechanical strength of the GNM/SWNT hybrid membrane can prevent tear and solute leakage to ensure robust water treatment over large areas.

Fabrication and structural characterization of GNM/SWNT hybrid membranes

Figure 2A shows the fabrication process of the GNM/SWNT hybrid membranes. Briefly, chemical vapor deposition (CVD)–grown single-layer graphene on Cu foil was used as the starting material. A layer of SWNT membrane consisting

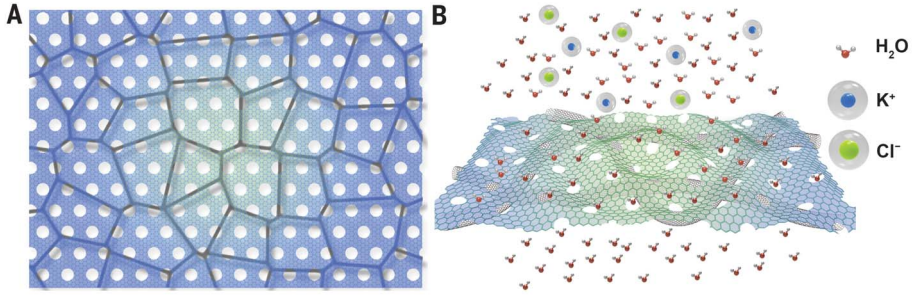

Fig. 1. Schematic illustration of the mechanically strong, large-area GNM/SWNT hybrid membrane for efficient water desalination. (**A**) Designed structural model of the GNM/SWNT hybrid membrane with single-layer GNM supported on SWNT networks. (**B**) Structural model of the GNM/SWNT hybrid membrane for size exclusion nanofiltration.

[1]College of Chemistry and Molecular Sciences, Key Laboratory of Analytical Chemistry for Biology and Medicine (Ministry of Education), Wuhan University, Wuhan 430072, China. [2]State Key Laboratory of Chemo/Biosensing and Chemometrics, College of Chemistry and Chemical Engineering, Hunan University, Changsha 410082, China. [3]Molecular Science and Biomedicine Laboratory, State Key Laboratory of Chemo/Biosensing and Chemometrics, College of Chemistry and Chemical Engineering, Hunan University, Changsha 410082, China. [4]Department of Engineering Science and Mechanics, The Pennsylvania State University, University Park, PA 16802, USA. [5]International Center for Materials Nanoarchitectonics (WPI-MANA), National Institute for Materials Science (NIMS), 1-1 Namiki, Tsukuba, Ibaraki 305-0044, Japan. [6]Department of Materials Science and Engineering, College of Engineering, Peking University, Beijing 100871, China. [7]Department of Chemistry and Biochemistry, University of California, Los Angeles, CA 90095, USA.
*These authors contributed equally to this work.
†Corresponding author. Email: yuanquan@whu.edu.cn (Q.Y.); xduan@chem.ucla.edu (X.D.)

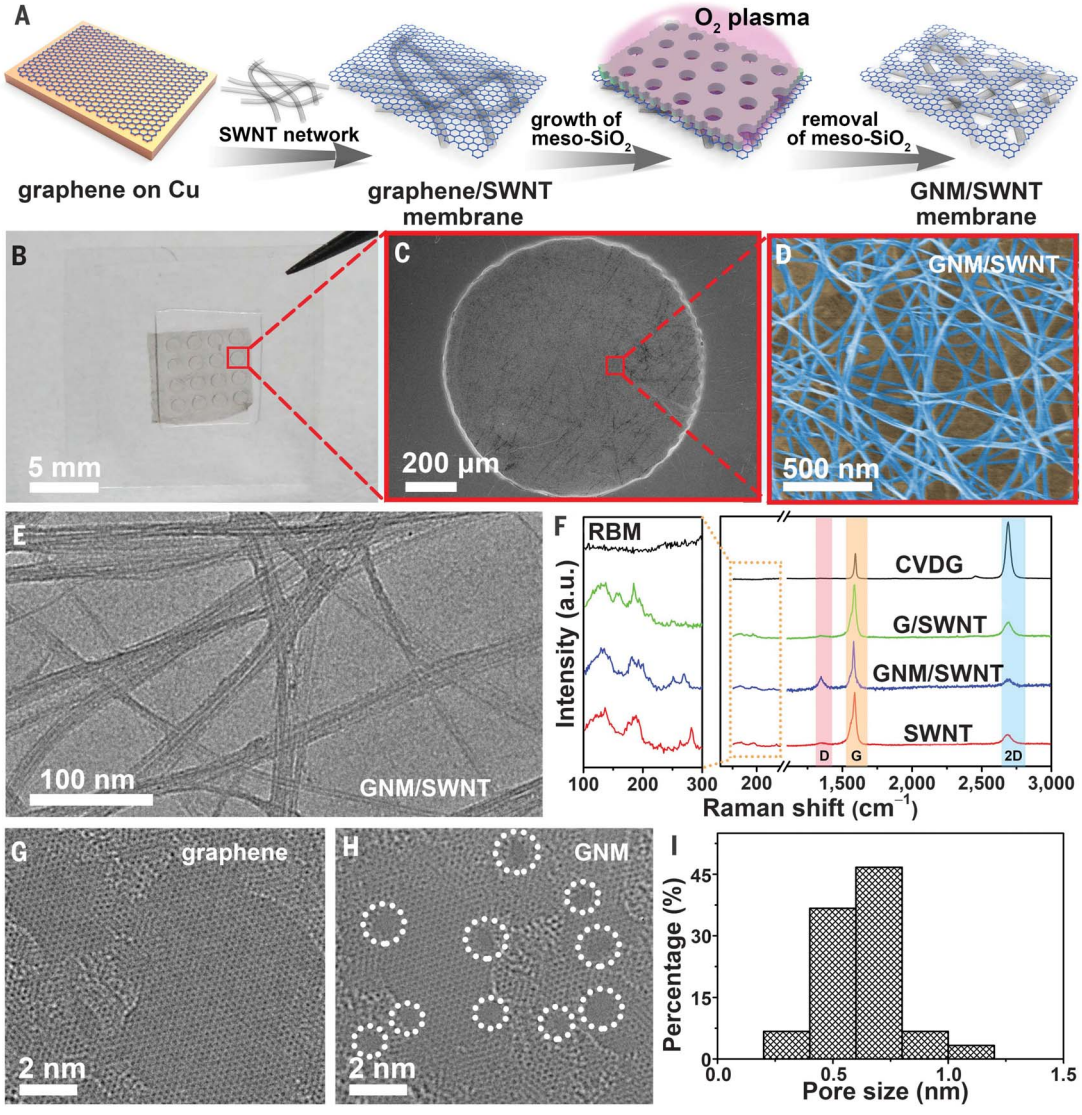

Fig. 2. Fabrication of GNM/SWNT hybrid membranes and structural characterizations. (**A**) Schematic illustration of the process used to fabricate GNM/SWNT hybrid membranes. (**B**) Photograph of the GNM/SWNT hybrid membrane suspended on a porous PDMS substrate with 16 holes (1 mm in diameter). (**C**) SEM image of a single hole in (B). (**D**) Magnified SEM image of the selected red area in (C). (**E**) TEM image of the GNM/SWNT hybrid membrane. (**F**) Raman spectra of CVDG, G/SWNT, GNM/SWNT, and SWNT membranes. (**G** and **H**) Aberration-corrected STEM image of graphene (G) and GNM (H) after 10 s of O_2 plasma etching. The white dashed circles highlight the pores present in GNM. (**I**) Pore-size distribution of the GNM prepared by 10 s of O_2 plasma etching.

of interconnected SWNTs was transferred on top of the graphene. After etching the Cu foils, a freestanding membrane with SWNT-supported graphene was obtained. To fabricate the GNM/SWNT membrane, we grew a layer of mesoporous SiO_2 (meso-SiO_2) film with uniform and perpendicular mesoporous channels (fig. S2) on the graphene surface as the porous template (*23*). By sequentially drilling pores in the graphene using O_2 plasma exposure and removing the meso-SiO_2 layer by hydrofluoric acid etching, we obtained a freestanding GNM/SWNT hybrid membrane, which can be suspended over a porous polydimethylsiloxane (PDMS) substrate. The suspended GNM/SWNT membrane retains the structural integrity with no obvious holes or tears (Fig. 2, B and C), as also confirmed by high-resolution scanning electron microscope (SEM) imaging (Fig. 2D). Transmission electron microscope (TEM) studies (Fig. 2E) further confirmed that the SWNT network intimately integrates with the GNM layer to form a mechanically strong, intact structure, whereas the pure graphene membrane readily cracks with obvious tears across the plane (fig. S3).

Raman spectroscopy was performed to evaluate the quality of the membranes. The pristine CVD-grown graphene (CVDG) showed clearly the characteristic 2D (2656 cm^{-1}) and G (1585 cm^{-1}) peaks with a high peak intensity ratio (I_{2D}/I_G~2) and no apparent D peak (1350 cm^{-1}) (Fig. 2F), suggesting that the pristine graphene exhibits a defect-free, single-layer characteristic. The presence of radial breathing modes at 100 to 300 cm^{-1} and the splitting of the G band confirm the existence of SWNTs in the graphene/SWNT (G/SWNT) membrane. After we introduced nanopores by O_2 plasma, the intensity of the D peak increased substantially to about one-third of that of the G peak (I_D/I_G~0.33) and the 2D peak intensity decreased, indicating the formation of defects in the GNM/SWNT membrane.

Scanning transmission electron microscopy (STEM) studies of the pristine graphene showed a honeycomb lattice of carbon atoms (Fig. 2G), whereas the STEM image of a GNM revealed the presence of subnanometer pores (Fig. 2H). The average pore size and pore density were

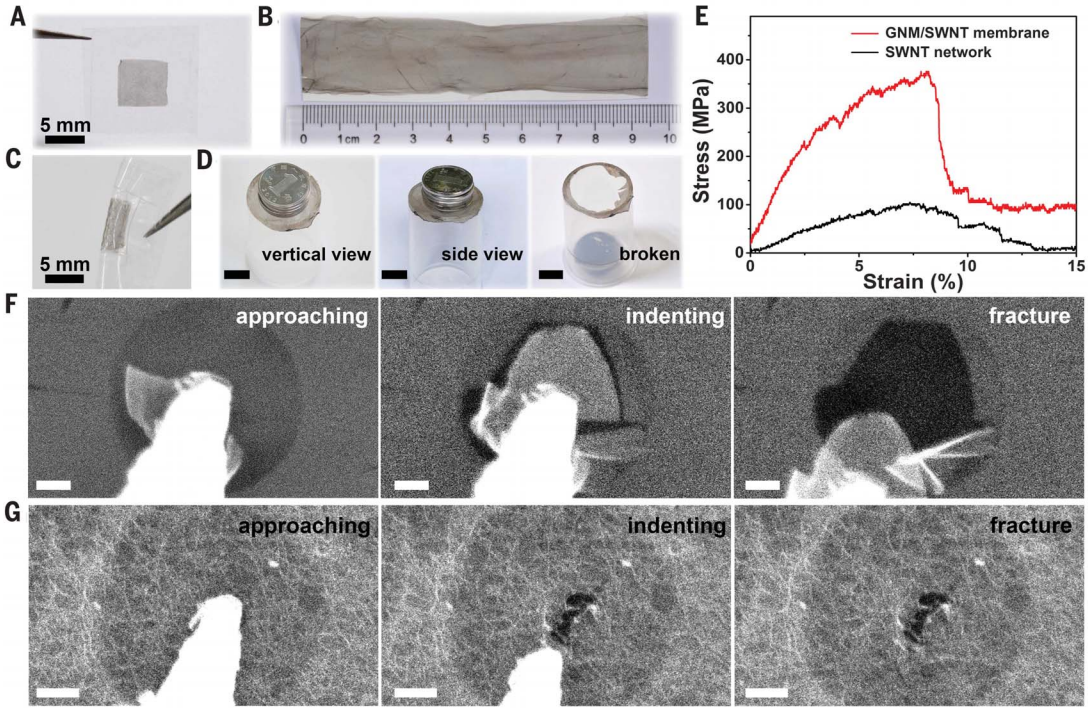

Fig. 3. Analysis of mechanical performance. (**A**) Photograph of the GNM/SWNT hybrid membrane suspended on a PET substrate with a 0.36-cm^2 hole. (**B**) Photograph of the large-area GNM/SWNT membrane. (**C**) Optical image of the GNM/SWNT hybrid membrane under bending conditions. (**D**) Photograph of the GNM/SWNT hybrid membrane suspended on a tube with six coins on the membrane. Scale bars, 1 cm. (**E**) Stress–strain curves of the SWNT membrane and the GNM/SWNT hybrid membrane under uniaxial tensile strain. (**F** and **G**) Rupture behavior of the (F) GNM and (G) GNM/SWNT hybrid membrane imaged by in situ SEM after poking with a micromanipulator. Scale bars, 0.5 μm (F) and 1 μm (G).

measured to be 0.63 nm and ~1.0 × 10^{12} cm^{-2}, respectively, in the GNM obtained with 10 s of O_2 plasma etching (Fig. 2I). The pore size matches well with the predicted optimal pore size for allowing water transport (0.32 nm) while effectively rejecting salt ions (~0.7 nm) (*17*). The pore size and pore density can be readily tailored by the O_2 plasma–etching time (fig. S4). A shorter etching time of 5 s results in an average pore size of ~0.55 nm, and an etching time of 20 s results in an average pore size of ~1.41 nm.

Mechanical characterization of GNM/SWNT hybrid membranes

The centimeter-scale GNM/SWNT hybrid membrane can be directly transferred onto a variety of substrates without a polymer support. A GNM/SWNT hybrid membrane suspended on a polyethylene terephthalate (PET) substrate with a 0.36-cm^2 square hole retains structural integrity without obvious cracks (Fig. 3A). The GNM/SWNT membrane may be readily scaled up (Fig. 3B) because there is no fundamental limitation in producing large-area graphene, the SWNT network, or meso-SiO_2 film up to meter scale. The flexible, freestanding SWNT network renders excellent mechanical strength and flexibility in the GNM/SWNT hybrid membrane, allowing it to endure large deformations without compromising the structural integrity (Fig. 3C). A hybrid membrane suspended on a tube edge is mechanically strong enough to support five coins (~16.0 g) without rupture (Fig. 3D).

We further investigated the tensile strength of the ultrathin GNM/SWNT hybrid membrane (*24*) (Fig. 3E and figs. S5 and S6). The SWNT and GNM/SWNT hybrid membranes showed similar fracture strains (8% and 9% for SWNT and GNM/SWNT membranes, respectively) (Fig. 3E). The pristine SWNT membrane could sustain a stress of 101.9 MPa (Fig. 3E) and the Young's modulus was calculated to be 2.6 GPa (fig. S7). By comparison, the GNM/SWNT membrane showed an enhanced mechanical strength to sustain a stress of 380.6 MPa (Fig. 3E) and had a considerably higher Young's modulus of 9.7 GPa (fig. S7). Additionally, atomic force microscope measurements indicated that the GNM/SWNT membrane has a modulus of ~5 to 10 GPa in the perpendicular direction (fig. S8). The mechanical strength is largely attributed to the Voronoi diagram structure of the GNM/SWNT network hybrid membrane, as confirmed by our mechanical simulations showing greatly enhanced tensile (2.4-fold) and bending stiffness (four orders of magnitude) of the GNM/SWNT membrane compared with the GNM membrane (figs. S9 to S12) (*24*).

In situ SEM imaging was conducted to visualize crack formation after punching a hole with a micromanipulator (Fig. 3, F and G). The GNM membrane quickly cracked into small pieces when a hole was punched. By contrast, the GNM/SWNT membrane maintained structural integrity during the entire process.

Water permeance and salt rejection under osmotic pressure

We explored the water-transport and salt-rejection properties of the GNM/SWNT hybrid membranes using three different configurations. The first configuration is based on cross-flow forward osmosis (FO) measurements in which the GNM/SWNT hybrid membrane suspended on a PET substrate (with a 0.16-cm^2 square aperture in the PET) separates two cavities, one filled with KCl solutions with different concentrations and the other with deionized water (Fig. 4A and fig. S13) (*24*). The osmotic pressure difference induced by the salt concentration gradient serves as the driving force for water transport. No apparent delamination between the SWNT network and the GNM membrane was observed in the cross-flow operation process or in the in situ SEM manipulations (Fig. 3G, fig. S14, and movie S1), confirming that the interaction between the SWNT and GNM is strong enough to resist the water flow under desalination conditions. On the basis of continuum mechanics, the maximum pressure (*P*) that a GNM/SWNT membrane with a pore size of 0.63 nm could withstand is calculated to be ~60 MPa (*24*) (Fig. 4B), consistent with previous theoretical calculations that the presence of a porous substrate (with openings <1 μm) would enable the GNM to sustain pressures exceeding 57 MPa (*19*). These analyses suggest that the GNM/SWNT hybrid membrane exhibits sufficient mechanical strength to be used as an effective semipermeable membrane for water desalination.

Water permeation studies showed that the G/SWNT membrane exhibits negligible water permeance (0.67 liter m^{-2} hour^{-1} bar^{-1}) (Fig. 4C and fig. S15), suggesting that the SWNT membrane maintains the structural integrity of graphene to prevent tearing and leakage. The water permeance for the GNM/SWNT hybrid membrane exhibits a clear dependence on the O_2 plasma–etching time (which correlates to the pore size). The GNM/SWNT membrane obtained with 5 s of etching (GNM/SWNT-5 s) showed a permeance of 7.5 liter m^{-2} hour^{-1} bar^{-1}. As the etching time was increased to 10 s (GNM/SWNT-10 s), the permeance increased to 20.6 liter m^{-2} hour^{-1}

bar^{-1} (5.7×10^{-16} g s^{-1} bar^{-1} per pore, assuming a pore density of 1.0×10^{12} cm^{-2}). This value is of the same order as that predicted by molecular dynamics simulations (*15*). A further increase of the etching time to 20 s (GNM/SWNT-20 s) resulted in a water permeance of 37.2 liter m^{-2} hour^{-1} bar^{-1}, indicating reduced transport resistance with increasing pore size in the GNM.

Compared with the water flux of the commercial cellulose triacetate (CTA) membrane, which becomes "self-limiting" at high salt concentrations, the water flux of the GNM/SWNT hybrid membrane showed a linear dependence versus the salt concentration (Fig. 4D and fig. S16), indicating that the internal concentration polarization (ICP) was nearly eliminated in the freestanding ultrathin GNM/SWNT membrane. The reduced osmotic pressure loss caused by ICP leads to a higher osmotic driving force and enhanced permeance.

The salt-rejection behavior was evaluated by measuring the salt permeance through the GNM/SWNT hybrid membrane (fig. S17). The salt permeance through the graphene/SWNT membrane was essentially zero (no transport of ions; Fig. 4C), suggesting that the graphene/SWNT membrane remains intact over large areas. The salt permeance of the GNM/SWNT membrane varied from 5.5 to 16.2 mol m^{-2} hour^{-1} when the O_2 plasma–etching time was increased from 5 to 20 s, indicating that the ion selectivity is highly dependent on the pore size. After 24 hours of permeation, the salt rejection for the GNM/SWNT membrane with 10 s of O_2 plasma–etching time remained >97% (Fig. 4E).

The separation performance of the GNM/SWNT membrane was also evaluated with NaCl as a seawater model. The measured salt rejection for NaCl was 98.1 ± 0.3% (fig. S18), which is comparable to that of KCl (97.1 ± 0.6%). The slightly improved salt rejection may be attributed to the relatively larger hydrated diameter of Na^+ (0.716 nm) compared with K^+ (0.662 nm). The minor salt leakage could be attributed to the presence of a small fraction of relatively large pores (~1 nm) in the GNM/SWNT membrane and the intrinsic defects or cracks formed during the graphene growth or transfer process. To this end, the presence of the SWNT network is particularly useful in separating the GNM into small domains and preventing the propagation of cracks and catastrophic failure.

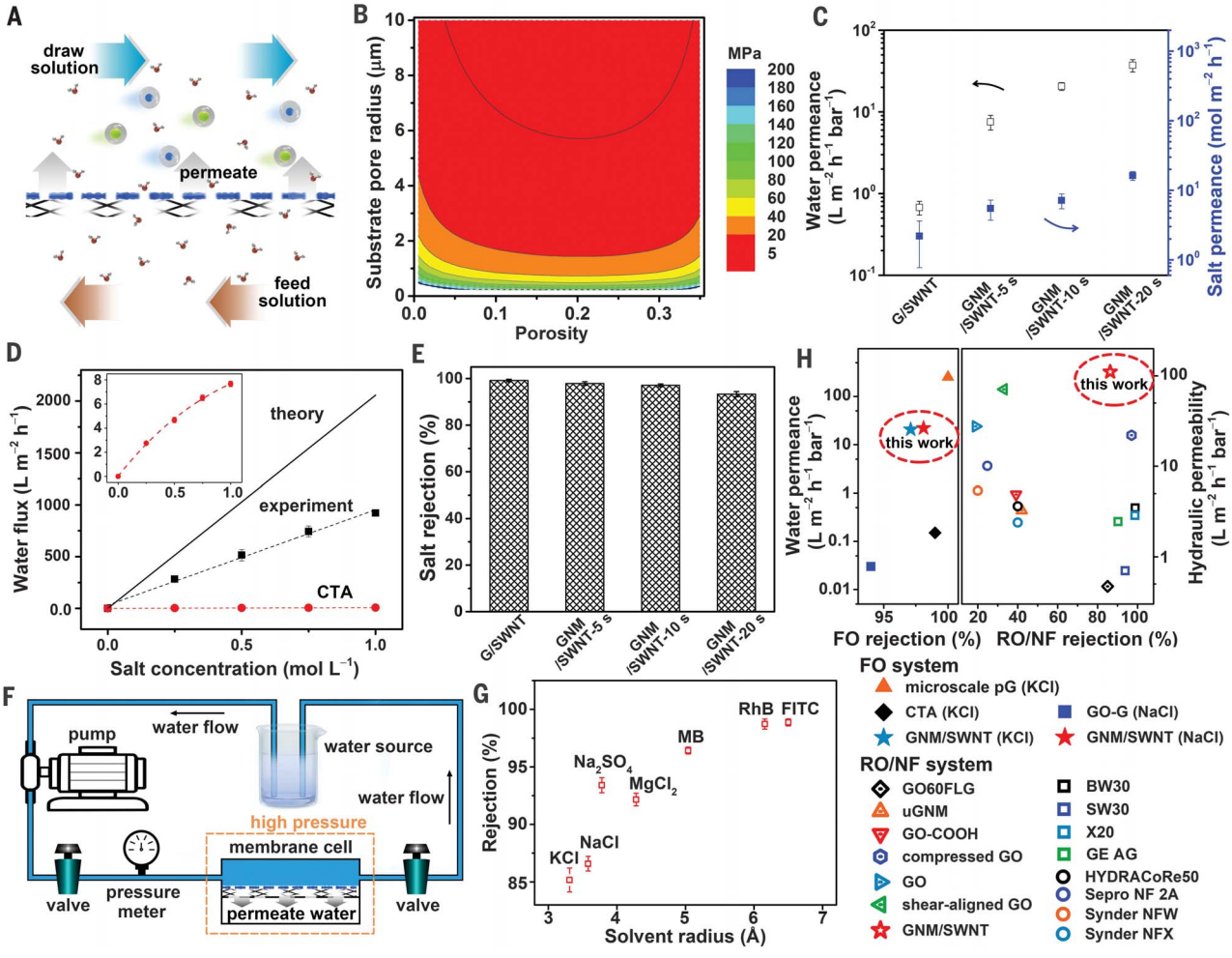

Fig. 4. Evaluation of water-desalination performance. (**A**) Sketch of water permeance through the GNM/SWNT membrane driven by osmotic pressure in the FO cross-flow system. (**B**) Contour plot of the maximum pressure versus GNM porosity and SWNT pore radius for GNM/SWNT-10 s. (**C**) Water and salt permeance through G/SWNT and GNM/SWNT membranes with O_2 plasma–etching times of 5, 10, and 20 s. (**D**) Water flux through the GNM/SWNT hybrid membrane and CTA membrane as a function of KCl concentration. Inset, the magnified view of the water flux of the CTA membrane. (**E**) Salt rejection of the G/SWNT and GNM/SWNT membranes prepared by O_2 plasma–etching times of 5, 10, and 20 s. (**F**) Schematic illustration of the RO cross-flow filtration apparatus. (**G**) Rejection of the GNM/SWNT membrane for KCl, NaCl, Na_2SO_4, $MgCl_2$, MB, RhB, and FITC. The error bars indicate the data acquired from three individual membranes. (**H**) Comparison of the water-permeability and salt-rejection performance of the GNM/SWNT hybrid membranes with commercial osmosis membranes and graphene-based separation membranes (*6*, *9*, *17*, *26*–*34*).

To further investigate the desalination performance of the GNM/SWNT membrane, we constructed a reverse osmosis (RO) cross-flow filtration apparatus (Fig. 4F) to measure the water- and salt-transport behaviors of the membrane toward Na_2SO_4, $MgCl_2$, NaCl, and KCl at a concentration of 2000 parts per million (ppm). As a nanofiltration membrane, the GNM/SWNT membrane could sustain a pressure in the range of ~2 to 4 MPa and ~8 to 10 MPa when supported by a stainless steel mesh (500 mesh, 30 μm pore size) and polycarbonate track etch membrane (0.2 μm pore size), suggesting that the GNM/SWNT membrane is mechanically strong enough to withstand typical commercial RO processes. The GNM/SWNT membrane showed high salt rejection between 85.2 and 93.4% (Fig. 4G), and the observed selectivity followed the order of Na_2SO_4 > $MgCl_2$ > NaCl > KCl. These observed salt-rejection ratios achieved in centimeter-scale GNM/SWNT membranes were generally smaller than those achieved in micrometer-scale nanoporous graphene flakes, which might be largely attributable to occasional defects or minor cracks in the large-area GNM/SWNT membranes. The hydraulic permeability of the GNM/SWNT membrane was maintained at 97.6 liters m^{-2} $hour^{-1}$ bar^{-1} for the NaCl solution compared with that of pure water (110.6 liters m^{-2} $hour^{-1}$ bar^{-1}) (fig. S19), further suggesting that the concentration polarization was effectively minimized. The increased membrane permeability could reduce the pressure necessary to drive efficient permeation and thus improve the energy efficiency of the desalination process. Additionally, the GNM/SWNT membrane exhibited higher water permeability and lower salt rejection in RO modules than in FO modules, and the exact reason for such differences is an intriguing topic for future investigations.

The GNM/SWNT membrane also exhibited a high rejection ratio for small charged or neutral molecules (96.4, 97.2, and 98.7% for methylene blue [MB], rhodamine B [RhB], and fluorescein isothiocyanate [FITC], respectively) with solvated diameters >1 nm (Fig. 4G and fig. S20), highlighting the merit of the GNM/SWNT membrane in rejecting small organic molecules, which is important for excluding small-molecule pharmaceuticals from drinking water, which typical commercial membranes usually fail to reject. The relatively high organic molecule exclusion performance and the decreased salt rejection with increasing Na_2SO_4 concentration (fig. S21) also suggest that the GNM/SWNT membrane is a nanofiltration membrane.

To gain further insight into the mechanism of salt rejection by the GNM/SWNT membrane, we also performed water-desalination measurements at different pH values. Little change was observed in salt rejection when the pH was varied from 7 to 3 (protonation of carboxylate groups at the pore edge), suggesting that the Gibbs–Donnan exclusion effect was negligible (figs. S22 to S24). Additionally, the GNM/SWNT membranes exhibited improved salt rejection for $MgCl_2$ (98.6%) compared with KCl (97.1%) (fig. S25) and an extremely low adsorption percentage (<0.5%; fig. S26) (*24*) for all of the investigated salts and organic molecules. These studies suggest that the salt-rejection performance of the GNM/SWNT membrane originates from (i) subnanometer-sized pores that facilitate effective separation by the size exclusion effect and (ii) the minimized concentration polarization due to the use of atomically thin nanoporous membrane in the cross-flow system.

We compared the permeability and selectivity of the GNM/SWNT water-desalination membranes with those reported in the literature (Fig. 4H and tables S1 and S2). The GNM/SWNT membrane exhibited a water permeance about one to two orders of magnitude higher than that of CTA, graphene oxide (GO)/graphene (*6*), and reduced GO membranes (*25*) at a comparable salt-rejection ratio. Nanoporous graphene (*17*) with high water permeance (252 liters m^{-2} $hour^{-1}$ bar^{-1}) has been reported previously, but only for micrometer-scale samples (10^{-6}–10^{-8} cm^2). Additionally, the GNM/SWNT membrane operated with the RO module showed about one to two orders of magnitude higher hydraulic permeability than that of commercial RO membranes, nanofiltration membranes, or graphene-based membranes (*9, 26–34*). The salt rejection of the GNM/SWNT membranes (>86% for NaCl) was lower than that for commercial RO membranes (90%~99%), but considerably higher than that for most graphene- or GO-based membranes (19 to 42%) (*26–29*) and commercial nanofiltration membranes (~24 to 40%) (*29, 33, 34*). The salt-rejection performance of the GNM/SWNT membranes could be further improved by optimizing the graphene growth conditions and the pore-formation process to minimize cracks and defects and to improve the pore size distribution.

The permeation and separation performance of our GNM/SWNT membranes was robust, and similar performance was observed in >100 studied membranes cut from large-area GNM/SWNT membranes. Compared with the CTA membrane, the GNM/SWNT membranes showed a high resistance to bacterial attachment for a long period of operation (figs. S27 and S28), indicating that the GNM/SWNT membranes exhibit excellent antibiofouling characteristics, which may be partly attributed to the smooth surface of the GNM (*35*) and the antibacterial performance of graphene (*36*).

Tubular water-desalination module

The commercial spiral-wound membranes are typically composed of stacked membranes scrolled into a tubular structure to enable a large contact area with feed solution and to further improve the water production output (*37*). Given the mechanical flexibility of the GNM/SWNT hybrid membranes, we investigated their water-desalination performance by bending the membrane to a specific curvature with a porous substrate (such as PDMS). The water-desalination device is composed of two stacked cylindrical silicone tubes, with the inner tube (0.16 cm^2 aperture present in the tube) incorporating a GNM/SWNT hybrid membrane (Fig. 5, A and B) (24). The control G/SWNT membrane exhibited negligible water and salt permeance that was nearly the same as that observed without bending (Fig. 5C and fig. S29), indicating that the G/SWNT membrane maintains the mechanical integrity well under bending conditions. The GNM/SWNT membrane showed a slight increase in permeance, by a factor of 1.2 and 1.6 for water and salt, respectively, indicating that the bending process may have induced the formation of a few small cracks. Despite the increased ion permeance, the GNM/SWNT membrane retained a salt rejection of up to 95.3% after 24 hours of osmotic operation (Fig. 5C), suggesting that the GNM/SWNT membrane is mechanically flexible enough to sustain

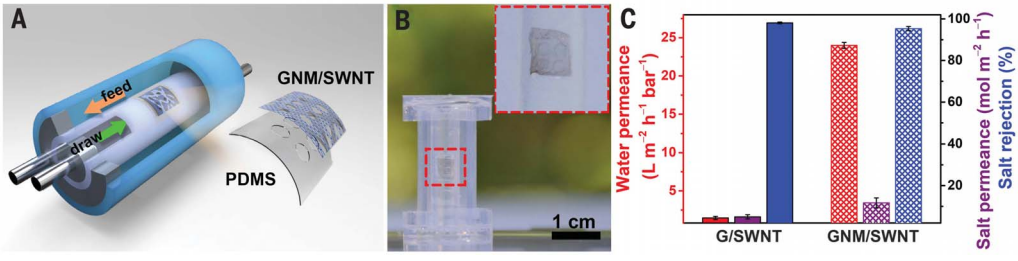

Fig. 5. Water-desalination performance of the bended membrane in a tubular module. (**A**) Schematic illustration and (**B**) photograph of the custom-assembled water-desalination cell for the measurement of permeance performance under bending conditions. Enlarged views show the corresponding structural model and photograph of the flexible GNM/SWNT membrane attached to the cylindrical silicone tube with a 0.16-cm^2 aperture. Scale bar, 1 cm. (**C**) Water and salt permeance and salt rejection of the G/SWNT and GNM/SWNT membranes under bending conditions. Error bars represent standard deviations of three independent measurements.

large deformation. The production efficiency can be further improved by packing the tubes incorporated with membranes into bundles with high packing density or scrolling the GNM/SWNT membrane into a spiral-wound structure. We further evaluated the water permeability and salt rejection of the GNM/SWNT membrane under different cross-flow velocities. The results indicated that the cross-flow velocity of 2 cm s^{-1} is the optimized condition for achieving high water permeance and salt rejection (fig. S30). At this velocity, the external concentration polarization is minimized while retaining sufficient membrane structural integrity.

We have designed a large-area, ultrathin GNM/SWNT hybrid membrane for highly efficient water purification. The macroscopic SWNT network helps to retain the structural integrity and improve the mechanical strength of monolayer GNM membrane, and the high-density subnanometer pores in the atomically thin GNMs ensure effective size-exclusion ionic/molecular nanofiltration and low permeation resistance. The GNM/SWNT hybrid membranes thus address the critical trade-off between water permeance and solute rejection in conventional desalination membranes. The high water permeance and excellent size selectivity combined with the excellent antifouling characteristics may make GNM/SWNT hybrid membranes highly attractive for energy-efficient and robust water treatment.

REFERENCES AND NOTES

1. A. Esfandiar *et al*., *Science* **358**, 511–513 (2017).
2. C. Klaysom, T. Y. Cath, T. Depuydt, I. F. J. Vankelecom, *Chem. Soc. Rev.* **42**, 6959–6989 (2013).
3. L.-C. Lin, J. C. Grossman, *Nat. Commun.* **6**, 8335 (2015).
4. S. Karan, Z. Jiang, A. G. Livingston, *Science* **348**, 1347–1351 (2015).
5. R. R. Nair, H. A. Wu, P. N. Jayaram, I. V. Grigorieva, A. K. Geim, *Science* **335**, 442–444 (2012).
6. J. Abraham *et al*., *Nat. Nanotechnol.* **12**, 546–550 (2017).
7. K. Goh *et al*., *Adv. Funct. Mater.* **25**, 7348–7359 (2015).
8. R. H. Tunuguntla *et al*., *Science* **357**, 792–796 (2017).
9. A. Morelos-Gomez *et al*., *Nat. Nanotechnol.* **12**, 1083–1088 (2017).
10. P. Sun, K. Wang, H. Zhu, *Adv. Mater.* **28**, 2287–2310 (2016).
11. J. Bai, X. Zhong, S. Jiang, Y. Huang, X. Duan, *Nat. Nanotechnol.* **5**, 190–194 (2010).
12. R. K. Joshi *et al*., *Science* **343**, 752–754 (2014).
13. B. Mi, *Science* **343**, 740–742 (2014).
14. L. Wang *et al*., *Nat. Nanotechnol.* **12**, 509–522 (2017).
15. D. Cohen-Tanugi, J. C. Grossman, *Nano Lett.* **12**, 3602–3608 (2012).
16. M. Heiranian, A. B. Farimani, N. R. Aluru, *Nat. Commun.* **6**, 8616 (2015).
17. S. P. Surwade *et al*., *Nat. Nanotechnol.* **10**, 459–464 (2015).
18. K. Celebi *et al*., *Science* **344**, 289–292 (2014).
19. D. Cohen-Tanugi, J. C. Grossman, *Nano Lett.* **14**, 6171–6178 (2014).
20. E. Shi *et al*., *Adv. Mater.* **27**, 682–688 (2015).
21. X. Lin *et al*., *Nat. Commun.* **4**, 2920 (2013).
22. J.-D. Boissonnat, F. Nielsen, R. Nock, *Discrete Comput. Geom.* **44**, 281–307 (2010).
23. Y. B. Yang *et al*., *Adv. Funct. Mater.* **27**, 1604096 (2017).
24. See supplementary materials.
25. H. Liu, H. Wang, X. Zhang, *Adv. Mater.* **27**, 249–254 (2015).
26. A. Akbari *et al*., *Nat. Commun.* **7**, 10891 (2016).
27. M. Hu, B. Mi, *Environ. Sci. Technol.* **47**, 3715–3723 (2013).
28. Y. Han, Z. Xu, C. Gao, *Adv. Funct. Mater.* **23**, 3693–3700 (2013).
29. Y. Q. Yuan *et al*., *Desalination* **405**, 29–39 (2017).
30. W. Li, W. Wu, Z. Li, *ACS Nano* **12**, 9309–9317 (2018).
31. W. Choi *et al*., *J. Membr. Sci.* **527**, 121–128 (2017).
32. Z. Jiang, S. Karan, A. G. Livingston, *Adv. Mater.* **30**, 1705973 (2018).
33. J. Y. Lin *et al*., *J. Membr. Sci.* **501**, 1–14 (2016).
34. Y.-J. Tang, Z.-L. Xu, S.-M. Xue, Y.-M. Wei, H. Yang, *J. Membr. Sci.* **498**, 374–384 (2016).
35. R. Yang, H. Jang, R. Stocker, K. K. Gleason, *Adv. Mater.* **26**, 1711–1718 (2014).
36. W. Hu *et al*., *ACS Nano* **4**, 4317–4323 (2010).
37. H. B. Park, J. Kamcev, L. M. Robeson, M. Elimelech, B. D. Freeman, *Science* **356**, eaab0530 (2017).

ACKNOWLEDGMENTS

Funding: We thank Y. Fang (National Center for Nanoscience and Technology, Beijing, China) for help with the synthesis of low-pressure CVD graphene. Q.Y. acknowledges support from the National Key Research and Development Program of China (2017YFA0208000), the National Natural Science Foundation of China (21675120), the Foundation for Innovative Research Groups of NSFC (21521063), the Ten Thousand Talents Program for Young Talents, the Start-up Research Fund (531107050973, 531109010053), and the State Key Laboratory of Chemo/Bio-Sensing and Chemometrics at Hunan University (734106172). H.C. is grateful for the start-up funds provided by The Pennsylvania State University. **Author contributions:** X.D., Q.Y., and A.C. proposed the research and supervised the project. Y.Y. and X.Y. designed and conducted the experiments and analyzed the experimental results. L.L. performed part of the structural characterization of the membranes. Y.G., H.C., X.L., and R.M. conducted the structural and simulation analysis of the membranes. M.Z. performed the growth of SWNT films and conducted the mechanical performance tests. Y.Y., X.Y., Q.Y., and X.D. cowrote the manuscript. All authors discussed the results and commented on the manuscript. **Competing interests:** The authors declare no competing interests. **Data and materials availability:** All data are available in the manuscript or in the supplementary materials.

SUPPLEMENTARY MATERIALS

science.sciencemag.org/content/364/6445/1057/suppl/DC1
Materials and Methods
Supplementary Text
Figs. S1 to S30
Tables S1 and S2
References (*38*–*51*)
Movie S1

20 June 2018; resubmitted 25 November 2018
Accepted 3 May 2019
10.1126/science.aau5321

Large-area graphene-nanomesh/carbon-nanotube hybrid membranes for ionic and molecular nanofiltration

Yanbing Yang, Xiangdong Yang, Ling Liang, Yuyan Gao, Huanyu Cheng, Xinming Li, Mingchu Zou, Renzhi Ma, Quan Yuan and Xiangfeng Duan

Science **364** (6445), 1057-1062.
DOI: 10.1126/science.aau5321

Supported graphene-based membranes

Porous graphene sheets have excellent filtration capabilities and are able to block most ions, but their fragility limits their scale-up beyond laboratory demonstrations. Yang *et al.* created a nanoporous graphene membrane reinforced by a network of single-walled carbon nanotubes (SWNTs) to provide mechanical stability (see the Perspective by Mi). The SWNT network also stopped the propagation of cracks in the graphene, effectively localizing the damage to a small area defined by a cell in the carbon nanotube mesh. The membranes showed high water flux rates as well as a high rejection rate for most ions.

Science, this issue p. 1057; see also p. 1033